Gravitational Constraints on the Earth's Inner Core Differential Rotation

Hugo Lecomte, Séverine Rosat, Mioara Mandea, Mathieu Dumberry

AGU ADVANCING EARTH AND SPACE SCIENCES

Geophysical Research Letters®

RESEARCH LETTER
10.1029/2023GL104790

Gravitational Constraints on the Earth's Inner Core Differential Rotation

Hugo Lecomte[1], Séverine Rosat[1], Mioara Mandea[2], and Mathieu Dumberry[3]

[1]Université de Strasbourg, CNRS, EOST, ITES UMR7063, Strasbourg, France, [2]Centre National d'Etudes Spatiales, Paris, France, [3]Department of Physics, University of Alberta, Edmonton, AB, Canada

Key Points:

- Satellite gravity observations restrict the range of possible values of the inner core (IC) rotation angle α and peak-to-peak topography δh
- The limits on the IC differential rotation rates are 0.16° yr^{-1}, 0.31° yr^{-1}, and 0.21° yr^{-1} at periods of ∼4, ∼6, and ∼12 years, for $\delta h = 90$ m
- Tighter values for α and δh can be obtained with a more accurate deconvolution of interannual hydrological effects from gravity data

Supporting Information:

Supporting Information may be found in the online version of this article.

Correspondence to:

H. Lecomte,
hugo.lecomte@univ-tlse3.fr

Citation:

Lecomte, H., Rosat, S., Mandea, M., & Dumberry, M. (2023). Gravitational constraints on the Earth's inner core differential rotation. *Geophysical Research Letters*, *50*, e2023GL104790. https://doi.org/10.1029/2023GL104790

Received 6 JUN 2023
Accepted 19 NOV 2023

Author Contributions:

Conceptualization: Séverine Rosat, Mioara Mandea
Data curation: Hugo Lecomte
Formal analysis: Hugo Lecomte
Funding acquisition: Séverine Rosat, Mioara Mandea, Mathieu Dumberry
Investigation: Hugo Lecomte, Mathieu Dumberry
Methodology: Hugo Lecomte, Séverine Rosat
Project Administration: Séverine Rosat, Mioara Mandea
Resources: Hugo Lecomte
Software: Hugo Lecomte

Abstract The differential axial rotation of the solid inner core (IC) is suggested by seismic observations and expected from core dynamics models. A rotation of the IC by an angle α takes its degree 2, order 2 topography (peak-to-peak amplitude δh) out of its gravitational alignment with the mantle. This creates a gravity variation of degree 2, order 2 proportional to δh and to α. Here, we use gravity observations from Satellite Laser Ranging, the Gravity Recovery and Climate Experiment (GRACE) and GRACE Follow-On to reconstruct the time-variable $S_{2,2}$ Stokes coefficient. We show that for $\delta h = 90$ m, $S_{2,2}$ provides upper bounds on α of 0.09°, 0.3°, and 0.4° at periods of ∼4, ∼6, and ∼12 years, respectively. These are overestimates, as our reconstructed $S_{2,2}$ signal likely remains polluted by hydrology, although viscous relaxation of the IC can permit larger amplitudes.

Plain Language Summary The inner core (IC) is the solid part of the core at Earth's center. The IC rotates together with the rest of the Earth, albeit with small fluctuations with respect to the mantle. These small variations are suggested by observations of seismic waves traversing the IC. The angle of change (α) of the peak-to-peak topography at the surface of the IC (δh) creates a change in the gravity field. By analyzing gravity variations recorded by satellites, we find upper limits on the possible values of α and δh. These constraints suggest that the angle of IC reorientation is no more than 0.4° at time periods between 4 and 12 years. Our results provide new constraints on the dynamics of the deepest part of our planet.

1. Introduction

The Earth's solid inner core (IC) is not expected to rotate synchronously with the mantle. On dynamical grounds, azimuthal (zonal) core flows (CF) close to the IC boundary (ICB) should, by electromagnetic coupling, exert a torque on the IC, and thereby alter its rotation rate (Gubbins, 1981). Observational evidences of this differential rotation have been reported by a number of seismic studies. The first of these were based on the travel time of seismic waves traversing the IC, in particular how this travel time changed over time, from which a mean eastward differential IC rotation rate of the order of 1° per year was inferred (Song & Richards, 1996; Su et al., 1996). Such rates were in line with predictions of the geodynamo numerical simulations emerging at that time (Glatzmaier & Roberts, 1996), in which a strong thermal wind flow near the ICB drove the IC into an eastward super-rotation.

These initial seismic results were challenged by a number of subsequent studies, using either different ray paths (Souriau, 2007; Zhang et al., 2005, 2008) or normal modes (Laske & Masters, 1999). The surface topography of a differentially rotating IC is taken out of its gravitational alignment with density anomalies in the mantle, resulting in a strong restoring gravitational torque opposing the driving electromagnetic torque (Buffett, 1996). A viscously deforming IC can still rotate differentially (Buffett, 1997), albeit at a much slower rate (Buffett & Glatzmaier, 2000). Extrapolation of dynamo simulation results to Earth-like conditions suggests a weak IC differential rotation, of the order of 1° per million years (Aubert & Dumberry, 2011).

However, CF vary on decadal and interannual timescales (Bloxham & Jackson, 1991; Gillet et al., 2022; Lesur et al., 2022). These should entrain fluctuations in the torque on the IC and changes in its rotation rate of the order of 0.1° per year (Dumberry, 2007) as seen in dynamo simulations (Aubert & Dumberry, 2011; Buffett & Glatzmaier, 2000). The more recent inferences of IC differential rotation from seismic observations tend to agree with these fluctuations (Wang & Vidale, 2022a; Yang & Song, 2022, 2023).

Supervision: Hugo Lecomte, Séverine Rosat
Validation: Hugo Lecomte, Mathieu Dumberry
Visualization: Hugo Lecomte
Writing – original draft: Hugo Lecomte, Séverine Rosat, Mioara Mandea
Writing – review & editing: Hugo Lecomte, Séverine Rosat, Mioara Mandea, Mathieu Dumberry

Here, for the first time, we set constraints on the fluctuating IC rotation by placing upper bounds on the azimuthal angle of rotation and its peak-to-peak topography from the degree 2, order 2 (hereafter noted (2,2)) gravity signal recorded by satellite gravimetry over the past 3 decades.

2. The Gravity Signal From an Oscillating Inner Core

Assuming hydrostatic equilibrium, the first order shape of the ICB should be an oblate ellipsoid with a mean radius $R_i = 1222$ km. Additional undulations of the ICB result from the IC hydrostatic adjustment to the gravitational potential imposed by mantle mass anomalies (including the core-mantle boundary (CMB) topography and other radial density discontinuities). These are dominated by a (2,2) signal connected to the large scale convective pattern in the mantle (e.g., Simmons et al., 2007). The IC distortion to adjust to this potential leads to a slightly elliptical ICB along the equator, with a peak-to-peak topography δh of the order of 100 m (e.g., Defraigne et al., 1996). Because of the ICB density contrast of $\Delta\rho_{ICB} = 600$ kg m^{-3} (Dziewonski & Anderson, 1981), decadal and interannual fluctuations of the IC rotation produce a (2,2) gravity variations and surface deformations (Dumberry & Mandea, 2022; Gillet et al., 2021). The amplitude of these signals depends on $\Delta\rho_{ICB}$, δh and the azimuthal angle of IC rotation, α (see Figure 1). While $\Delta\rho_{ICB}$ is relatively well constrained (Gubbins et al., 2008; Tkalčić et al., 2009), estimates of δh and α are less certain.

The gravitational potential $V(\theta, \phi)$ at co-latitude θ and longitude ϕ at the Earth's surface (mean radius $R = 6.371 \times 10^6$ m) is expressed in a spherical harmonic expansion as

$$V(\theta,\phi) = -\frac{GM}{R}\left[\sum_{l=0}^{\infty}\sum_{m=0}^{l}(C_{l,m}\cos m\phi + S_{l,m}\sin m\phi)\bar{P}_{l,m}(\cos\theta)\right], \tag{1}$$

where $M = 5.972 \times 10^{24}$ kg is the Earth's mass, G is the gravitational constant, $C_{l,m}$ and $S_{l,m}$ are the (dimensionless) Stokes coefficients, and $\bar{P}_{l,m}(\cos\theta)$ are normalized associated Legendre polynomials, related to the regular (unnormalized) associated Legendre polynomials $P_{l,m}(\cos\theta)$ by

$$\bar{P}_{l,m}(\cos\theta) = \left[(2-\delta_{m0})(2l+1)\frac{(l-m)!}{(l+m)!}\right]^{1/2} P_{l,m}(\cos\theta), \tag{2}$$

where δ_{m0} is the Kronecker delta.

Let us assume the IC is an elastic solid with a uniform density, and with a (2,2) topography expressed as

$$h(\theta,\phi) = \left(h^c_{2,2}\cos 2\phi + h^s_{2,2}\sin 2\phi\right)\bar{P}_{2,2}(\cos\theta). \tag{3}$$

The coefficients $h^c_{2,2}$ and $h^s_{2,2}$ are connected to α by,

$$h^c_{2,2} = \frac{\delta h}{\sqrt{15}}\cos 2\alpha, \qquad h^s_{2,2} = \frac{\delta h}{\sqrt{15}}\sin 2\alpha, \tag{4}$$

where δh is the peak-to-peak amplitude of the topography along the equator. The surface mass density $\Delta\rho_{ICB} \times h(\theta, \phi)$ associated with this topography generates a gravitational potential signal at the surface of

$$C_{2,2} = (1+\kappa_2)\frac{4\pi}{5}\frac{R_i^4}{R^2}\frac{\Delta\rho_{ICB}}{M}h^c_{2,2}, \qquad S_{2,2} = (1+\kappa_2)\frac{4\pi}{5}\frac{R_i^4}{R^2}\frac{\Delta\rho_{ICB}}{M}h^s_{2,2}, \tag{5}$$

where the Love number $\kappa_2 = 0.9736$ accounts for the additional gravity signal resulting from global elastic deformations (Dumberry, 2008).

Let us write $\alpha = \alpha_o + \alpha(t)$, where α_o is the fixed orientation of the IC with respect to the mantle and $\alpha(t)$ its temporally varying part induced by fluctuations in its axial rotation rate. The change in Stokes coefficients induced by $\alpha(t)$ is

$$\Delta C_{2,2} = \mathcal{K}\delta h[\cos(2\alpha_o + 2\alpha(t)) - \cos(2\alpha_o)], \tag{6a}$$

$$\Delta S_{2,2} = \mathcal{K}\delta h[\sin(2\alpha_o + 2\alpha(t)) - \sin(2\alpha_o)], \tag{6b}$$

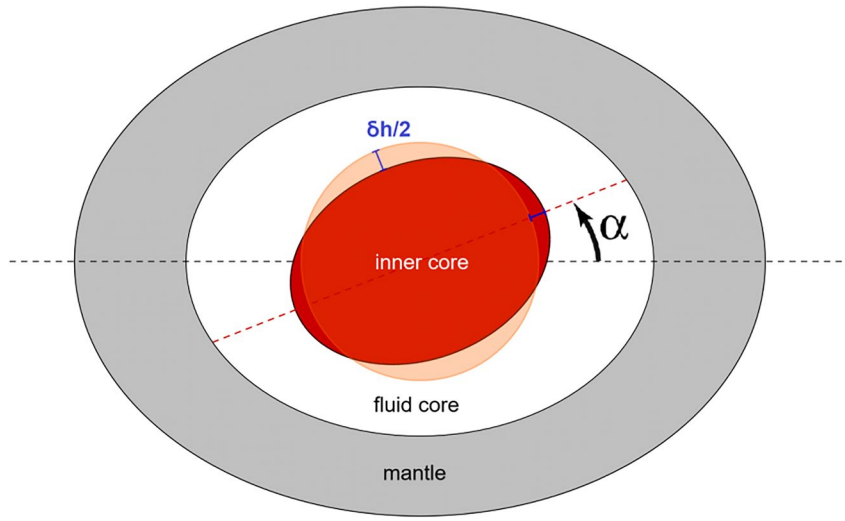

Figure 1. Equatorial cross-section of the Earth with an azimuthal rotation α of the inner core (IC) with respect to the longitude 0°. The IC possesses an equatorial ellipsoidal shape represented in blue by half of the peak-to-peak δh topography. Adapted from Dumberry and Mandea (2022) and not drawn at scale.

where

$$\mathcal{K} = (1+\kappa_2)\frac{4\pi}{5\sqrt{15}}\frac{R_i^4}{R^2}\frac{\Delta\rho_{ICB}}{M} = 7.07\times10^{-12}. \tag{6c}$$

The fixed IC orientation α_o depends on the orientation of the (2,2) topography of the gravitational potential (geoid) at the CMB induced by convective mantle mass anomalies. This orientation is not known precisely, but models suggest that it is generally aligned with longitude 0° (e.g., Defraigne et al., 1996). For simplicity, let us assume that $\alpha_o = 0°$. Given the low rates of differential IC rotation predicted on dynamical grounds (~0.1° yr^{-1}), $\alpha(t)$ should remain small for fluctuations at a timescale shorter than a few decades. For $\alpha_o = 0°$ and $\alpha(t) \ll 1$, Equations 6a and 6b simplify to

$$\Delta C_{2,2} = \mathcal{K}\,\delta h[\cos(2\alpha(t)) - 1] \simeq -2\,\mathcal{K}\,\delta h\,\alpha(t)^2, \tag{7a}$$

$$\Delta S_{2,2} = \mathcal{K}\,\delta h\,\sin(2\alpha(t)) \simeq 2\,\mathcal{K}\,\delta h\,\alpha(t). \tag{7b}$$

Provided $\alpha(t)$ remains small, $\Delta S_{2,2}$ is much larger than $\Delta C_{2,2}$. Let us take $\delta h = 100$ m and $\alpha = 1°$, this gives $\Delta S_{2,2} \approx 2.5\times10^{-11}$ and $\Delta C_{2,2} \approx 4.3\times10^{-13}$. If the time-averaged IC orientation α_o is not zero, the difference in amplitude between $\Delta S_{2,2}$ and $\Delta C_{2,2}$ is reduced. The expression for $\Delta S_{2,2}$ in Equation 7b gives the best upper bound for the (2,2) gravity signal.

For a rigid IC, $\alpha(t)$ is equal to the angular rotation of the IC bulk, the quantity which is measured seismically, that we denote by $\phi(t)$. If the ICB topography relaxes viscously in a characteristic time τ toward its equilibrium alignment with the mantle, then (Buffett, 1997)

$$\frac{d\alpha}{dt} = \frac{d\phi}{dt} - \frac{\alpha}{\tau}. \tag{8}$$

When τ is comparable or smaller than the timescale of the fluctuations of interest, $\phi(t)$ and $\alpha(t)$ differ, and the bulk rotates at a faster rate than the ICB topography. The upper bound that we obtain from Equation 7b is on α, not ϕ. To simplify, we assume a rigid IC, so that $\alpha(t) \equiv \phi(t)$. However, larger values of bulk IC rotation are allowed if the ICB relaxes viscously (see Discussions).

3. Previous Estimates of α and δh

Previous estimates of α come from a combination of seismic studies, CF reconstructions and considerations of core-mantle angular momentum exchanges. These estimates were presented in Dumberry and Mandea (2022)

but are reproduced and updated here. Estimates of δh are based on mass anomalies in the mantle deduced from seismic tomography and geodynamical models.

3.1. α From Zonal Core Flows

Time-varying zonal flows at the CMB can be reconstructed from the secular variation of the geomagnetic field (Bloxham & Jackson, 1991; Holme, 2015). On decadal timescales and shorter, zonal flows are expected to be invariant along the direction of the rotation axis (Gillet et al., 2011; Jault, 2008); zonal flows at the ICB should be the axial projection of the zonal flows at the CMB. Electromagnetic coupling at the ICB is expected to be sufficiently strong (Gubbins, 1981) that the IC should be entrained into co-rotation with the mean zonal flows. Assuming small oscillation amplitudes, the relation between the ICB zonal flows, v_ϕ, and the IC rotation angle α at frequency ω is $v_\phi = R_i\,\omega\,\alpha$.

CF models suggest fluctuations in CMB zonal flow with an amplitude of approximately 0.4 km yr^{-1} at a 6-year period and approximately 2 km yr^{-1} at a 30-year period (Gillet et al., 2019, 2021). These give indirect estimates of $\alpha \approx 0.018°$ and $\alpha \approx 0.4°$ at periods of 6 and 30 years, respectively.

3.2. α From Length of Day (LOD) Variations

Decadal (Holme & de Viron, 2013; Jault et al., 1988) and interannual (Gillet et al., 2010, 2022) variations in the Length of Day (LOD) results from core-mantle angular momentum exchanges. The nature of the torque between the core and the mantle remains not well known, but if gravitational coupling is entirely responsible for the observed LOD changes (ΔLOD), the latter can be used to predict α (Buffett & Creager, 1999):

$$\alpha = -\frac{2\pi}{T_o^2}\frac{C_m}{\Gamma}\frac{d}{dt}\Delta\mathrm{LOD}, \tag{9}$$

where T_o is the Earth's rotation period (T_o = 86400 s), C_m is the polar moment of inertia of the mantle ($C_m = 7.129 \times 10^{37}$ kg m^2) and Γ represents the constant net gravitational torque between the mantle and the IC. Estimates of Γ can be constructed based on mantle density anomalies inferred from seismic tomography models and viscous mantle flow models and range from 3×10^{19} to 2×10^{20} N m (Davies et al., 2014).

In Text S1 in Supporting Information S1, we show that the amplitude of the observed LOD changes over the past 70 years with periods longer than 20 years are approximately 1 ms. For the lower and upper bounds of Γ, this translates to amplitudes of α between 0.6° and 0.09°. At 6-year, ΔLOD $\approx$ 0.2 ms corresponding to amplitudes of α between 0.7° and 0.1°.

3.3. α From Seismic Waves

For earthquake doublets, the temporal shift of the wave envelope can be mapped to a change in α. Using this approach, Zhang et al. (2005) and Tkalčić et al. (2013) propose a differential rotation rate of 0.25°–0.5° yr^{-1} with a fluctuation over a period of approximately 20 years. This corresponds to an amplitude of α = [0.25–0.5]° yr^{-1} $\times \frac{20}{2\pi}$ yr $\approx$ [0.8–1.6]°. Yang and Song (2023) suggest a history of IC differential rotation that includes a 65-year period of amplitude $\alpha \simeq 2.5°$, with a minimum of ~4° in the early 1970s and a maximum of ~1° in 2009. Wang and Vidale (2022a) find a rotation rate of 0.1° yr^{-1} between 1971 and 1974 which they interpret as a 6-year signal with an amplitude $\alpha \simeq 0.2°$ (Wang & Vidale, 2022b).

3.4. δh From Seismic Tomography and Geodynamic Models

Mass anomalies involved in mantle convection distort the surfaces of gravitational potential from the CMB to ICB. If we assume that the IC viscous deformation timescale is smaller than that of the mantle, the ICB topography (averaged over time) should coincide with the undulations of the gravitational potential at the ICB (Buffett, 1997). The latter is connected to its undulations at the CMB (Dumberry, 2010; Wahr & de Vries, 1989). The CMB gravitational potential, in turn, may be computed from geodynamic models, in particular by combining mantle density anomalies inferred from seismic tomography, the mantle viscous flow that they produce, and using the observed surface geoid as an additional constraint (e.g., Defraigne et al., 1996; Simmons et al., 2007). Values for δh are estimated using geodynamic models at some 70 m by Defraigne et al. (1996) or in the range of

[49–126] m estimated from $\Gamma = [3 \times 10^{19} - 2 \times 10^{20}]$ N m (Davies et al., 2014). We summarize the various δh ranges in Text S2 in Supporting Information S1.

An alternative modeling approach is to assume that the 6-year period in LOD changes is caused by the free mode of mantle-IC gravitational oscillation. When the whole of the tangent cylinder is assumed to follow the IC, the value of Γ must be approximately 3×10^{20} N m (Davies et al., 2014). This corresponds to $\delta h \simeq 154$ m, in agreement with an independent calculation by Shih and Chao (2021). We note, however, that this assumes that the angular momentum exchange at a 6-year period is between the mantle and the IC, yet observations suggest that it is instead between the mantle and the fluid core (Gillet et al., 2010).

4. Data and Method

The Gravity Recovery and Climate Experiment (GRACE) and GRACE Follow-On (GRACE-FO) satellite missions deliver time-variable gravity measurements since 2002 (Landerer et al., 2020; Tapley et al., 2004). Satellite Laser Ranging (SLR) measures the time variation of the (2,2) gravity field coefficients since the 1980s (Löcher & Kusche, 2020a). The observed (2,2) signal contains contributions from different sources: tidal deformations, post-glacial rebound (Purcell et al., 2011), hydrological (Rodell et al., 2018), atmospheric and oceanic loading (Dobslaw et al., 2017), water mass displacement and exchanges between ocean, hydrosphere and cryosphere (Pfeffer et al., 2022), sea level changes (Adhikari et al., 2019), mantle mass redistribution (Panet et al., 2018), and core processes (Dumberry & Mandea, 2022). To access the signal originating from the core, the signals from all other sources must be removed. This is a challenge as models for the planetary-scale mass fluctuations induced by surface processes remain incomplete (Pfeffer et al., 2022).

We use $S_{2,2}$ from the product IGG-SLR-HYBRID Ensemble Mean (referred as IGG-SLR) (Löcher & Kusche, 2020a). This product takes advantage of the temporal length of the SLR time-series and the qualities of GRACE(-FO). The formal errors provided with IGG-SLR are unrealistic as too optimistic. This $S_{2,2}$ series is the mean of solutions based on SLR measurements only and on GRACE(-FO) empirical orthogonal functions (EOFs) from the ITSG-Grace2018 product (Mayer-Gürr et al., 2018) and spans from November 1992 to December 2020. The longest well resolved oscillation period (i.e., two complete cycles) is then 14 years (Sundararajan, 2023).

The EOFs are cleared of sub-monthly surface loading aliasing (Dobslaw et al., 2017), hydrological loading at longer periods and Earth's interior mass redistribution are not corrected. The $S_{2,2}$ series in the IGG-SLR solution is similar to that of the GRACE products from 3 different analysis centers (Text S3 in Supporting Information S1).

To reduce the hydrological contribution from $S_{2,2}$ variations we use a global hydrological model obtained independently from gravitational observations. Interaction Sol-Biosphère-Atmosphère CNRM version of TRIP (ISBA-CTRIP, henceforth referred to as ISBA) solves the vertical water mass balance and the lateral fluxes to

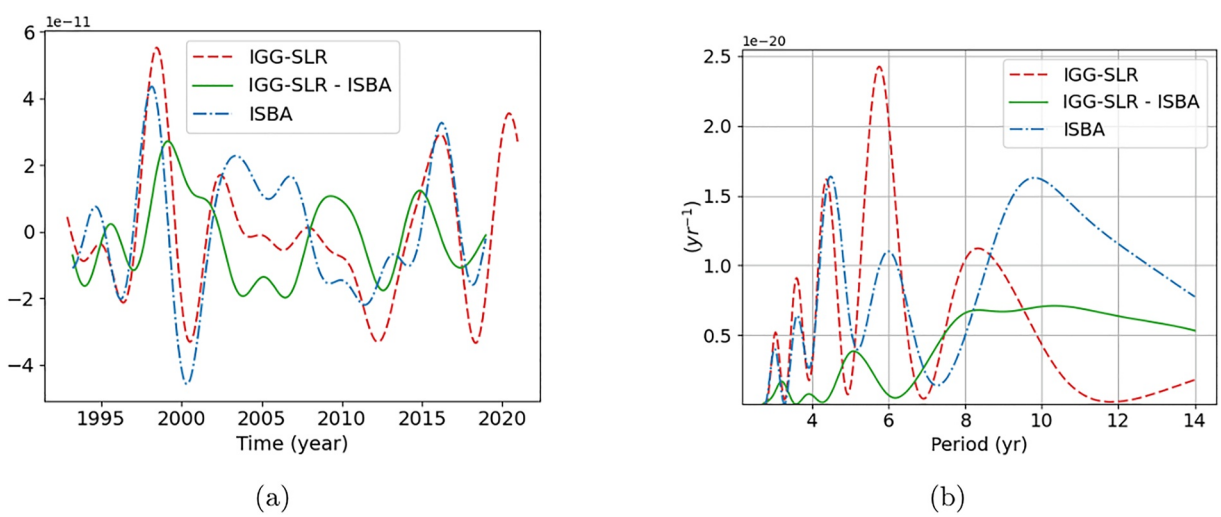

Figure 2. (a) Time-series and (b) Lomb-Scargle periodogram of $S_{2,2}$ coefficient for IGG-SLR (red) product, IGG-SLR minus ISBA combination (green), and ISBA (blue), with *y*-axis scale at the top-left.

model hydrological loading variations (Decharme et al., 2019). ISBA is available from 1979 to December 2018. ISBA explains the low degrees interannual gravity signals observed by GRACE better than other hydrological models (Lecomte et al., 2023).

Figure 2a shows the time-series of $S_{2,2}$ from the IGG-SLR product, the ISBA model, and what we refer to henceforth as the corrected $S_{2,2}$ signal (ISBA subtracted from IGG-SLR). Their associated periodograms are shown in Figure 2b. To access interannual timescales, we have applied a low-pass filter with a cut-off period of 3 years, and used a Hamming window to reduce the apodization effect. The IGG-SLR time-series contains large signals at periods of 4.5, 5.8, and 8.6 years. The 5.8-year peak is dominantly caused by the large oscillation between 1998 and 2002 that is also present in the ISBA model (Figure 2a) and therefore corresponds to a hydrological signal. After the correction with the ISBA model, the corrected time-series spectral content is reduced with one peak at 5 years, a plateau between 8 and 14 years and the standard deviation of $S_{2,2}$ is reduced by 32%.

Periods of 5.8 and 8.6 years have already been identified in the LOD time-series (Duan & Huang, 2020) and in CF models (Rosat & Gillet, 2023). These signals are then typically assumed to originate from CF processes. However, given the fit between the gravity variations and the ISBA hydrological model at similar periods (Figure 2a), the influence of surface processes on the LOD cannot be discounted. In a more general perspective, a 6-year oscillation appears to involve the whole Earth's system, a signal whose origin is still unexplained (Cazenave et al., 2023).

5. Results

Although surface processes contribute to a part of the corrected $S_{2,2}$ time-series (Lecomte et al., 2023), it potentially contains a signature of the IC reorientation. Figure 3 shows the temporal evolution of α implied by the corrected $S_{2,2}$ time-series based on Equation 7b for δh values in the range 49–126 m (Davies et al., 2014). These α time-series are based on the assumption that all residual variations are attributable to the IC reorientation, which is unrealistic since a contribution from surface processes likely remains.

The corrected $S_{2,2}$ time-series periodogram (Figure 2b) allows us to place upper bounds for three ranges of periods: the peak at 4 years with an amplitude of 2×10^{-12}, the peak between 5 and 6 years with an amplitude of 7×10^{-12}, and the plateau between 8 and 12 years with an amplitude of 9×10^{-12}. For an assumed $\delta h = 90$ m, approximately the mid-point of the range 49–126 m, the corresponding upper bounds on α are 0.09°, 0.3°, and 0.4°, respectively. These represent generous upper bounds because the corrected $S_{2,2}$ time-series likely contain unremoved hydrological effects (Pfeffer et al., 2022). These upper bounds are summarized in Table 1, together with estimates from other observations; the upper bounds on α without applying the hydrological correction are significantly larger (first line of Table 1).

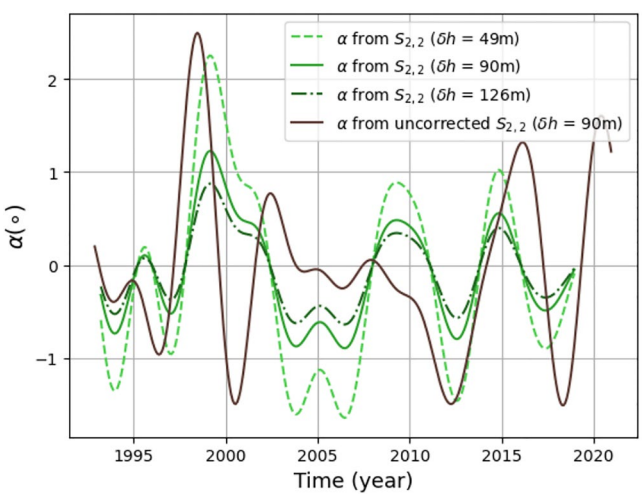

Figure 3. α time-series reconstructed from Equation 7b based on the corrected $S_{2,2}$ variations (green) for different choices of δh (49, 90, and 126 m) and based on the $S_{2,2}$ time-series uncorrected for hydrological loading with $\delta h = 90$ m (brown).

An upper bound on $S_{2,2}$ translates to upper bounds on the combination of α and δh, as shown in Figure 4. The three colored curves represent the upper bound constraints for the same periods as those highlighted in Table 1. For a given period range and a choice of δh, $S_{2,2}$ observations limit the upper bound of α to be below the shown curves. A smaller choice of δh allows for a larger α upper bound; conversely, a larger δh restricts α to a smaller upper bound.

6. Discussions and Conclusions

We present a new constraint on the amplitude of the IC axial reorientation angle α based on the observed time-variable gravity field $S_{2,2}$ Stokes coefficient. Using the $S_{2,2}$ time-series corrected for hydrology, α must be smaller than 0.09°, 0.3°, and 0.4° at periods of 4, 5–6, and 8–12 years, respectively. For a rigid IC, these correspond to maximum IC differential rotation rates of 0.16° yr^{-1}, 0.31° yr^{-1}, and 0.21° yr^{-1}, respectively. These upper bounds on α assume a peak-to-peak (2,2) ICB topography of $\delta h = 90$ m and that no other processes contribute to the corrected $S_{2,2}$ signal. Although we have reduced the hydrological contribution from the $S_{2,2}$ series, it is likely that some hydrological effects remain (Pfeffer et al., 2022). Indeed, the $C_{2,2}$ variation

Table 1
Upper Bound Values of α Based on the $S_{2,2}$ Time-Series and for δh = 90 m Compared With Estimates From Other Observations

Observation	Period (years) 4	5–6	8–12	20–30	References
IGG-SLR	0.7°	0.8°	0.6°		This paper
IGG-SLR - ISBA	0.09°	0.3°	0.4°		This paper
Zonal flows		0.018°		0.4°	Gillet et al. (2021)
LOD		0.1°–0.7°		0.09°–0.6°	Buffett and Creager (1999) and Davies et al. (2014)
Seismic rays		0.2°		0.8°–1.6°	Tkalčić et al. (2013) and Zhang et al. (2005)

Note. The LOD estimate is built from Buffett and Creager (1999) theory and Davies et al. (2014) results, but is not reported in these studies.

amplitudes (Text S4 in Supporting Information S1) are not substantially different from those of $S_{2,2}$, hinting that hydrological processes dominate the (2,2) observed gravity signal. If so, the true upper limits on α are smaller.

Our study is important in light of recent seismic inferences of the changes in α. Wang and Vidale (2022b) estimate a change of $\alpha = -0.1°$ between 1969 and 1971 and a change of $\alpha = 0.29°$ between 1971 and 1974. They further show that this matches the prediction reconstructed from the 6-year oscillation in LOD. In the hypothesis that the latter is purely due to IC-mantle gravitational coupling (Text S1 in Supporting Information S1), the inferred 6-year fluctuation amplitude ($\alpha \approx 0.2°$) is below our derived upper bound, but would not be if more than one third of our corrected $S_{2,2}$ series remains polluted by hydrology.

Another key factor to consider is the IC viscosity, allowing the ICB topography of the axially rotated IC to partly relax viscously back into an alignment with the gravitational potential imposed by mantle mass anomalies (Buffett, 1997). Mineral physics suggest viscosity values between 10^{16} and 10^{18} Pa s (e.g., Gleason & Mao, 2013; Ritterbex & Tsuchiya, 2020) and nutation observations values as small as 10^{14} Pa s (Koot & Dumberry, 2011), much smaller than the mantle viscosity. This corresponds to a range of viscous relaxation timescales of $\tau = 0.002$–20 years (Buffett, 1997). Ensuring that the IC-mantle gravitational coupling does not lead to decadal LOD changes that exceed observations yields an upper bound on τ of 1–6 years (Davies et al., 2014). Taking viscous relaxation into account, the bulk IC rotation (ϕ) is connected to the ICB topography change α by Equation 8. Our upper bounds for the bulk IC rotation are increased by a factor $\sqrt{(\omega\tau)^2 + 1}/(\omega\tau)$, where ω is the oscillation frequency. The upper bound on the bulk IC rotation can increase when $\omega\tau$ is comparable to or smaller than 1. For example, at a 6-year period, our upper bound is multiply by 1.4 for $\tau = 1$ year, and by 9.6 for $\tau = 0.1$ year.

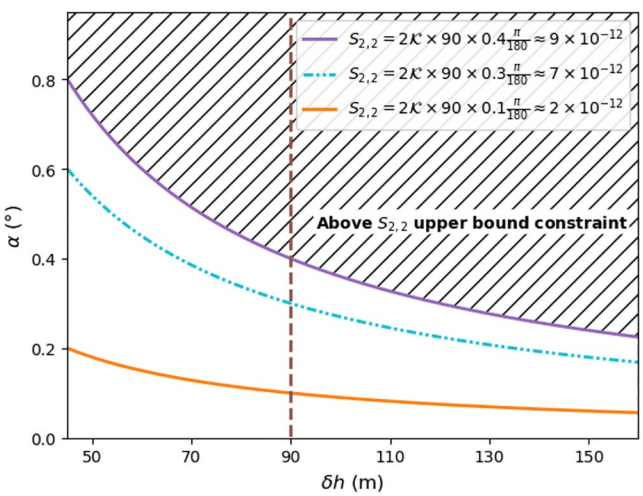

Figure 4. Upper bounds on the combination of α and δh for periods of ∼4 (orange curve), ∼6 (blue curve), and ∼12 (purple curve) years, based on the corrected $S_{2,2}$ signal amplitudes (2×10^{-12}, 7×10^{-12}, and 9×10^{-12}, respectively). The brown dotted line corresponds to the assumption $\delta h = 90$ m used for the calculations shown in the legend and for the upper bounds on α given in Table 1. The hatched area corresponds to values of δh and α not allowed by the observed $S_{2,2}$ signal.

Our study illustrates that the gravity signal of (2,2) offers a complementary way to reconstruct the IC differential rotation. Future improvements in the gravity record itself and in hydrological loading models will provide a more accurate $S_{2,2}$ determination. Not only this will bring a firmer upper bound for α, but it may eventually enable to detect the actual time variations of α from gravimetry.

Acronyms

CMB	Core-Mantle Boundary
CNES	Centre National d'Études Spatiales
CSR	Center for Space Research
EOF	Empirical Orthogonal Functions
EOP	Earth Orientation Parameters
GFZ	German Research Centre for Geosciences
GIA	Glacial Isostatic Adjustment
GRACE	Gravity Recovery And Climate Experiment
GRACE-FO	Gravity Recovery And Climate Experiment Follow-On

GRAZ	Institute of Geodesy at Graz University of Technology
ICB	Inner-Core Boundary
IERS	International Earth Rotation and Reference System Service
ISBA	Interaction Sol-Biosphère-Atmosphère
ISBA-CTRIP	Interaction Sol-Biosphère-Atmosphère CNRM version of TRIP
LOD	Length Of Day
SLR	Satellite Laser Ranging
WGHM	WaterGAP Global Hydrology Model

Data Availability Statement

GRACE and GRACE-FO missions are sponsored by the National Aeronautics and Space Administration and the Deutsches Zentrum für Luft-und Raumfahrt. GRACE and GRACE-FO Level-2 temporal solutions were obtained from icgem.gfz-potsdam.de for the IGG-SLR product (Löcher & Kusche, 2020b), COST-G (Meyer et al., 2020), and the GRAZ center (Mayer-Gürr et al., 2018). CSR center products were downloaded from the PO.DAAC Drive (CSR RL6.0, 2018). The ISBA-CTRIP model made by the "Centre National de Recherches Météorologiques" (CNRM) of Météo-France has been provided by Bertrand Decharmes (Decharme et al., 2019).

Code Availability Statement: The Python 3.8 code used for this publication is based on a Github project by Tyler Tsutterley https://github.com/tsutterley/read-GRACE-harmonics, licensed under MIT (Sutterley, 2023). The adapted version can be found on https://github.com/hulecom/read-GRACE-harmonics repository. After installation of the library (adapted version) and download of the data, the Python notebook "GRL_Gravitational_Lecomte2023b.ipynb" available in the repository allows to reproduce the figures of this article.

Acknowledgments
This work is supported by the Centre National d'Études Spatiales (CNES) and by the Doctoral School Earth and Environmental Sciences (ED 413) of the University of Strasbourg in the Institut Terre et Environnement de Strasbourg (ITES, CNRS UMR7063). This project has received funding from the European Research Council (ERC) under the European Union's Horizon 2020 research and innovation program (GRACEFUL Synergy Grant 855677). This work was supported by CNES, focused on GRACE and on Geodesy. MD is supported by a Discovery Grant from NSERC/CRSNG. We thank to the editor Lucy Flesch and the referees for their valuable inputs and remarks which helped us to improve this paper.

References

Adhikari, S., Ivins, E. R., Frederikse, T., Landerer, F. W., & Caron, L. (2019). Sea-level fingerprints emergent from GRACE mission data. *Earth System Science Data*, *11*(2), 629–646. https://doi.org/10.5194/essd-11-629-2019

Aubert, J., & Dumberry, M. (2011). Steady and fluctuating inner core rotation in numerical geodynamo models. *Geophysical Journal International*, *184*(1), 162–170. https://doi.org/10.1111/j.1365-246x.2010.04842.x

Bloxham, J., & Jackson, A. (1991). Fluid flow near the surface of Earth's outer core. *Reviews of Geophysics*, *29*(1), 97–120. https://doi.org/10.1029/90rg02470

Buffett, B. A. (1996). Gravitational oscillations in the length of day. *Geophysical Research Letters*, *23*(17), 2279–2282. https://doi.org/10.1029/96GL02083

Buffett, B. A. (1997). Geodynamic estimates of the viscosity of the Earth's inner core. *Nature*, *388*(6642), 571–573. https://doi.org/10.1038/41534

Buffett, B. A., & Creager, K. C. (1999). A comparison of geodetic and seismic estimates of inner-core rotation. *Geophysical Research Letters*, *26*(10), 1509–1512. https://doi.org/10.1029/1999GL900271

Buffett, B. A., & Glatzmaier, G. A. (2000). Gravitational braking of inner-core rotation in geodynamo simulations. *Geophysical Research Letters*, *27*(19), 3125–3128. https://doi.org/10.1029/2000gl011705

Cazenave, A., Pfeffer, J., Mandea, M., & Dehant, V. (2023). A 6-year oscillation in the whole Earth system? *Earth System Dynamics Ideas*, *14*(4), 733–735. https://doi.org/10.5194/esd-14-733-2023

CSR RL6.0. (2018). Grace field geopotential coefficients CSR release 6.0 [Dataset]. Stl. Retrieved from https://podaac.jpl.nasa.gov/dataset/GRACE_GSM_L2_GRAV_CSR_RL06

Davies, C. J., Stegman, D. R., & Dumberry, M. (2014). The strength of gravitational core-mantle coupling. *Geophysical Research Letters*, *41*(11), 3786–3792. https://doi.org/10.1002/2014GL059836

Decharme, B., Delire, C., Minvielle, M., Colin, J., Vergnes, J.-P., Alias, A., et al. (2019). Recent changes in the ISBA-CTRIP land surface system for use in the CNRM-CM6 climate model and in global off-line hydrological applications. *Journal of Advances in Modeling Earth Systems*, *11*(5), 1207–1252. https://doi.org/10.1029/2018MS001545

Defraigne, P., Dehant, V., & Wahr, J. M. (1996). Internal loading of an inhomogeneous compressible Earth with phase boundaries. *Geophysical Journal International*, *125*(1), 173–192. https://doi.org/10.1111/j.1365-246x.1996.tb06544.x

Dobslaw, H., Bergmann-Wolf, I., Dill, R., Poropat, L., Thomas, M., Dahle, C., et al. (2017). A new high-resolution model of non-tidal atmosphere and ocean mass variability for de-aliasing of satellite gravity observations: AOD1B RL06. *Geophysical Journal International*, *211*(1), 263–269. https://doi.org/10.1093/gji/ggx302

Duan, P., & Huang, C. (2020). Intradecadal variations in length of day and their correspondence with geomagnetic jerks. *Nature Communications*, *11*(1), 2273. https://doi.org/10.1038/s41467-020-16109-8

Dumberry, M. (2007). Geodynamic constraints on the steady and time-dependent inner core axial rotation. *Geophysical Journal International*, *170*(2), 886–895. https://doi.org/10.1111/j.1365-246x.2007.03484.x

Dumberry, M. (2008). Decadal variations in gravity caused by a tilt of the inner core. *Geophysical Journal International*, *172*(3), 921–933. https://doi.org/10.1111/j.1365-246x.2007.03624.x

Dumberry, M. (2010). Gravitationally driven inner core differential rotation. *Earth and Planetary Science Letters*, *297*(3–4), 387–394. https://doi.org/10.1016/j.epsl.2010.06.040

Dumberry, M., & Mandea, M. (2022). Gravity variations and ground deformations resulting from core dynamics. *Surveys in Geophysics*, *43*(1), 5–39. https://doi.org/10.1007/s10712-021-09656-2

Dziewonski, A., & Anderson, D. (1981). Preliminary reference Earth model. *Physics of the Earth and Planetary Interiors*, *25*(4), 297–356. https://doi.org/10.1016/0031-9201(81)90046-7

Gillet, N., Dumberry, M., & Rosat, S. (2021). The limited contribution from outer core dynamics to global deformations at the Earth's surface. *Geophysical Journal International*, *224*(1), 216–229. https://doi.org/10.1093/gji/ggaa448

Gillet, N., Gerick, F., Jault, D., Schwaiger, T., Aubert, J., & Istas, M. (2022). Satellite magnetic data reveal interannual waves in Earth's core. *Proceedings of the National Academy of Sciences*, *119*(13), e2115258119. https://doi.org/10.1073/pnas.2115258119

Gillet, N., Huder, L., & Aubert, J. (2019). A reduced stochastic model of core surface dynamics based on geodynamo simulations. *Geophysical Journal International*, *219*(1), 522–539. https://doi.org/10.1093/gji/ggz313

Gillet, N., Jault, D., Canet, E., & Fournier, A. (2010). Fast torsional waves and strong magnetic field within the Earth's core. *Nature*, *465*(7294), 74–77. https://doi.org/10.1038/nature09010

Gillet, N., Schaeffer, N., & Jault, D. (2011). Rationale and geophysical evidence for quasi-geostrophic rapid dynamics within the Earth's outer core. *Physics of the Earth and Planetary Interiors*, *187*(3), 380–390. https://doi.org/10.1016/j.pepi.2011.01.005

Glatzmaier, G. A., & Roberts, P. H. (1996). Rotation and magnetism of Earth's inner core. *Science*, *274*(5294), 1887–1891. https://doi.org/10.1126/science.274.5294.1887

Gleason, A. E., & Mao, W. L. (2013). Strength of iron at core pressures and evidence for a weak Earth's inner core. *Nature Geoscience*, *6*(7), 571–574. https://doi.org/10.1038/ngeo1808

Gubbins, D. (1981). Rotation of the inner core. *Journal of Geophysical Research*, *86*(B12), 11695–11699. https://doi.org/10.1029/JB086iB12p11695

Gubbins, D., Masters, G., & Nimmo, F. (2008). A thermochemical boundary layer at the base of Earth's outer core and independent estimate of core heat flux. *Geophysical Journal International*, *174*(3), 1007–1018. https://doi.org/10.1111/j.1365-246X.2008.03879.x

Holme, R. (2015). Large-scale flow in the core. In G. Schubert & P. Olson (Eds.), *Treatise on geophysics* (Vol. 8, pp. 91–113). Elsevier.

Holme, R., & de Viron, O. (2013). Characterization and implications of intradecadal variations in length of day. *Nature*, *499*(7457), 202–204. https://doi.org/10.1038/nature12282

Jault, D. (2008). Axial invariance of rapidly varying diffusionless motions in the Earth's core interior. *Physics of the Earth and Planetary Interiors*, *166*(1), 67–76. https://doi.org/10.1016/j.pepi.2007.11.001

Jault, D., Gire, C., & Le Mouël, J.-L. (1988). Westward drift, core motions and exchanges of angular momentum between core and mantle. *Nature*, *333*(6171), 353–356. https://doi.org/10.1038/333353a0

Koot, L., & Dumberry, M. (2011). Viscosity of the Earth's inner core: Constraints from nutation observations. *Earth and Planetary Science Letters*, *308*(3), 343–349. https://doi.org/10.1016/j.epsl.2011.06.004

Landerer, F. W., Flechtner, F. M., Save, H., Webb, F. H., Bandikova, T., Bertiger, W. I., et al. (2020). Extending the global mass change data record: GRACE follow-on instrument and science data performance. *Geophysical Research Letters*, *47*(12), e2020GL088306. https://doi.org/10.1029/2020GL088306

Laske, G., & Masters, G. (1999). Limits on differential rotation of the inner core from an analysis of the Earth's free oscillations. *Nature*, *402*(6757), 66–69. https://doi.org/10.1038/47011

Lecomte, H., Rosat, S., Mandea, M., Boy, J.-P., & Pfeffer, J. (2023). Uncertainty of low-degree space gravimetry observations: Surface processes versus internal signal. *Journal of Geophysical Research: Solid Earth*, *128*(7), e2023JB026503. https://doi.org/10.1029/2023jb026503

Lesur, V., Gillet, N., Hammer, M. D., & Mandea, M. (2022). Rapid variations of Earth's core magnetic field. *Surveys in Geophysics*, *43*(1), 41–69. https://doi.org/10.1007/s10712-021-09662-4

Löcher, A., & Kusche, J. (2020a). A hybrid approach for recovering high-resolution temporal gravity fields from satellite laser ranging. *Journal of Geodesy*, *95*(1), 6. https://doi.org/10.1007/s00190-020-01460-x

Löcher, A., & Kusche, J. (2020b). IGG_SLR_HYBRID [Dataset]. ICGEM. Retrieved from http://icgem.gfz-potsdam.de/series/10.1007/s00190-020-01460-x

Mayer-Gürr, T., Behzadpur, S., Ellmer, M., Kvas, A., Klinger, B., Strasser, S., & Zehentner, N. (2018). *ITSG-Grace2018 - Monthly, daily and static gravity field solutions from GRACE*. GFZ Data Services.

Meyer, U., Jaeggi, A., Dahle, C., Flechtner, F., Kvas, A., Behzadpour, S., et al. (2020). *International combination Service for time-variable gravity fields (COST-G) monthly GRACE series*. GFZ Data Services. https://doi.org/10.5880/ICGEM.COST-G.001

Panet, I., Bonvalot, S., Narteau, C., Remy, D., & Lemoine, J.-M. (2018). Migrating pattern of deformation prior to the Tohoku-Oki earthquake revealed by GRACE data. *Nature Geoscience*, *11*(5), 367–373. https://doi.org/10.1038/s41561-018-0099-3

Pfeffer, J., Cazenave, A., Blazquez, A., Decharme, B., Munier, S., & Barnoud, A. (2022). Detection of slow changes in terrestrial water storage with GRACE and GRACE-FO satellite gravity missions. *EGUsphere*, 1–85. https://doi.org/10.5194/egusphere-2022-1032

Purcell, A., Dehecq, A., Tregoning, P., Potter, E.-K., McClusky, S. C., & Lambeck, K. (2011). Relationship between glacial isostatic adjustment and gravity perturbations observed by GRACE. *Geophysical Research Letters*, *38*(18), L18305. https://doi.org/10.1029/2011GL048624

Ritterbex, S., & Tsuchiya, T. (2020). Viscosity of hcp iron at Earth's inner core conditions from density functional theory. *Scientific Reports*, *10*(1), 6311. https://doi.org/10.1038/s41598-020-63166-6

Rodell, M., Famiglietti, J. S., Wiese, D. N., Reager, J. T., Beaudoing, H. K., Landerer, F. W., & Lo, M.-H. (2018). Emerging trends in global freshwater availability. *Nature*, *557*(7707), 651–659. https://doi.org/10.1038/s41586-018-0123-1

Rosat, S., & Gillet, N. (2023). Intradecadal variations in length of day: Coherence with models of the Earth's core dynamics. *Physics of the Earth and Planetary Interiors*, *341*, 107053. https://doi.org/10.1016/j.pepi.2023.107053

Shih, S. A., & Chao, B. F. (2021). Inner core and its libration under gravitational equilibrium: Implications to lower-mantle density anomaly. *Journal of Geophysical Research: Solid Earth*, *126*(1), e2020JB020541. https://doi.org/10.1029/2020JB020541

Simmons, N. A., Forte, A. M., & Grand, S. P. (2007). Thermochemical structure and dynamics of the African superplume. *Geophysical Research Letters*, *34*(2), L02301. https://doi.org/10.1029/2006gl028009

Song, X. D., & Richards, P. G. (1996). Seismological evidence for differential rotation of the Earth's inner core. *Nature*, *382*(6588), 221–224. https://doi.org/10.1038/382221a0

Souriau, A. (2007). Deep Earth structure - The Earth's cores. In *Treatise on geophysics* (Vol. 1, pp. 655–693). Elsevier.

Su, W. J., Dziewonski, A. M., & Jeanloz, R. (1996). Planet within a planet: Rotation of the inner core of the Earth. *Science*, *274*(5294), 1883–1887. https://doi.org/10.1126/science.274.5294.1883

Sundararajan, D. (2023). *Signals and systems: A practical approach*. Springer Nature Switzerland. https://doi.org/10.1007/978-3-031-19377-4

Sutterley, T. (2023). Tsutterley/gravity-toolkit: V1.2.1 [Software]. Zenodo. https://doi.org/10.5281/zenodo.8075728

Tapley, B. D., Bettadpur, S., Ries, J. C., Thompson, P. F., & Watkins, M. M. (2004). GRACE measurements of mass variability in the Earth system. *Science*, *305*(5683), 503–505. https://doi.org/10.1126/science.1099192

Tkalčić, H., Kennett, B. L. N., & Cormier, V. F. (2009). On the inner—Outer core density contrast from PKiKP/PcP amplitude ratios and uncertainties caused by seismic noise. *Geophysical Journal International*, *179*(1), 425–443. https://doi.org/10.1111/j.1365-246X.2009.04294.x

Tkalčić, H., Young, M., Bodin, T., Ngo, S., & Sambridge, M. (2013). The shuffling rotation of the Earth's inner core revealed by earthquake doublets. *Nature Geoscience*, *6*(6), 497–502. https://doi.org/10.1038/ngeo1813

Wahr, J., & de Vries, D. (1989). The possibility of lateral structure inside the core and its implications for nutation and Earth tide observations. *Geophysical Journal International*, *99*(3), 511–519. https://doi.org/10.1111/j.1365-246x.1989.tb02036.x

Wang, W., & Vidale, J. E. (2022a). Earth's inner core rotation, 1971 to 1974, illuminated by inner-core scattered waves. *Earth and Planetary Science Letters*, *577*, 117214. https://doi.org/10.1016/j.epsl.2021.117214

Wang, W., & Vidale, J. E. (2022b). Seismological observation of Earth's oscillating inner core. *Science Advances*, *8*(23), eabm9916. https://doi.org/10.1126/sciadv.abm9916

Yang, Y., & Song, X. (2022). Inner core rotation captured by earthquake doublets and twin stations. *Geophysical Research Letters*, *49*(12), e2022GL098393. https://doi.org/10.1029/2022GL098393

Yang, Y., & Song, X. (2023). Multidecadal variation of the Earth's inner-core rotation. *Nature Geoscience*, *16*(2), 1–6. https://doi.org/10.1038/s41561-022-01112-z

Zhang, J., Richards, P. G., & Schaff, D. P. (2008). Wide-scale detection of earthquake waveform doublets and further evidence for inner core super-rotation. *Geophysical Journal International*, *174*(3), 993–1006. https://doi.org/10.1111/j.1365-246X.2008.03856.x

Zhang, J., Song, X., Li, Y., Richards, P. G., Sun, X., & Waldhauser, F. (2005). Inner core differential motion confirmed by earthquake waveform doublets. *Science*, *309*(5739), 1357–1360. https://doi.org/10.1126/science.1113193

References From the Supporting Information

Bizouard, C. (2020). *Geophysical modelling of the polar motion*. Walter de Gruyter GmbH & Co KG.

Dobslaw, H., & Dill, R. (2018). Predicting earth orientation changes from global forecasts of atmosphere-hydrosphere dynamics. *Advances in Space Research*, *61*(4), 1047–1054. https://doi.org/10.1016/j.asr.2017.11.044

Rekier, J., Chao, B. F., Chen, J., Dehant, V., Rosat, S., & Zhu, P. (2022). Earth's rotation: Observations and relation to deep interior. *Surveys in Geophysics*, *43*(1), 149–175. https://doi.org/10.1007/s10712-021-09669-x